The Astrophysical Journal, 664:397–410, 2007 July 20

SEARCH FOR NEUTRINO-INDUCED CASCADES FROM GAMMA-RAY BURSTS WITH AMANDA

A. Achterberg,[1] M. Ackermann,[2] J. Adams,[3] J. Ahrens,[4] K. Andeen,[5] J. Auffenberg,[6] J. N. Bahcall,[7,8] X. Bai,[9] B. Baret,[10] S. W. Barwick,[11] R. Bay,[12] K. Beattie,[13] T. Becka,[4] J. K. Becker,[14] K.-H. Becker,[6] P. Berghaus,[15] D. Berley,[16] E. Bernardini,[2] D. Bertrand,[15] D. Z. Besson,[17] E. Blaufuss,[16] D. J. Boersma,[5] C. Bohm,[18] J. Bolmont,[2] S. Böser,[2] O. Botner,[19] A. Bouchta,[19] J. Braun,[5] C. Burgess,[18] T. Burgess,[18] T. Castermans,[20] D. Chirkin,[13] B. Christy,[16] J. Clem,[9] D. F. Cowen,[21,22] M. V. D'Agostino,[12] A. Davour,[19] C. T. Day,[13] C. De Clercq,[10] L. Demirörs,[9] F. Descamps,[23] P. Desiati,[5] T. DeYoung,[21] J. C. Diaz-Velez,[5] J. Dreyer,[14] J. P. Dumm,[5] M. R. Duvoort,[1] W. R. Edwards,[13] R. Ehrlich,[16] J. Eisch,[24] R. W. Ellsworth,[16] P. A. Evenson,[9] O. Fadiran,[25] A. R. Fazely,[26] K. Filimonov,[12] M. M. Foerster,[21] B. D. Fox,[21] A. Franckowiak,[6] T. K. Gaisser,[9] J. Gallagher,[27] R. Ganugapati,[5] H. Geenen,[6] L. Gerhardt,[11] A. Goldschmidt,[13] J. A. Goodman,[16] R. Gozzini,[4] T. Griesel,[4] S. Grullon,[5] A. Groß,[28] R. M. Gunasingha,[26] M. Gurtner,[6] A. Hallgren,[19] F. Halzen,[5] K. Han,[3] K. Hanson,[5] D. Hardtke,[12] R. Hardtke,[24] J. E. Hart,[21] Y. Hasegawa,[29] T. Hauschildt,[9] D. Hays,[13] J. Heise,[1] K. Helbing,[6] M. Hellwig,[4] P. Herquet,[20] G. C. Hill,[5] J. Hodges,[5] K. D. Hoffman,[16] B. Hommez,[23] K. Hoshina,[5] D. Hubert,[10] B. Hughey,[5] P. O. Hulth,[18] K. Hultqvist,[18] J.-P. Hülß,[30] S. Hundertmark,[18] M. Inaba,[29] A. Ishihara,[29] J. Jacobsen,[13] G. S. Japaridze,[25] H. Johansson,[18] A. Jones,[13] J. M. Joseph,[13] K.-H. Kampert,[6] T. Karg,[6] A. Karle,[5] H. Kawai,[29] J. L. Kelley,[5] N. Kitamura,[5] S. R. Klein,[13] S. Klepser,[2] G. Kohnen,[20] H. Kolanoski,[31] L. Köpke,[4] M. Kowalski,[31] T. Kowarik,[4] M. Krasberg,[5] K. Kuehn,[11] M. Labare,[15] H. Landsman,[5] H. Leich,[2] D. Leier,[14] I. Liubarsky,[32] J. Lundberg,[19] J. Lünemann,[14] J. Madsen,[24] K. Mase,[29] H. S. Matis,[13] T. McCauley,[13] C. P. McParland,[13] A. Meli,[14] T. Messarius,[14] P. Mészáros,[21,22] H. Miyamoto,[29] A. Mokhtarani,[13] T. Montaruli,[5,33] A. Morey,[12] R. Morse,[5] S. M. Movit,[22] K. Münich,[14] R. Nahnhauer,[2] J. W. Nam,[11] P. Nießen,[9] D. R. Nygren,[13] H. Ögelman,[5] A. Olivas,[16] S. Patton,[13] C. Peña-Garay,[7] C. Pérez de los Heros,[19] A. Piegsa,[4] D. Pieloth,[2] A. C. Pohl,[19,34] R. Porrata,[12] J. Pretz,[16] P. B. Price,[12] G. T. Przybylski,[13] K. Rawlins,[35] S. Razzaque,[21,22] E. Resconi,[28] W. Rhode,[14] M. Ribordy,[20] A. Rizzo,[10] S. Robbins,[6] P. Roth,[16] C. Rott,[21] D. Rutledge,[21] D. Ryckbosch,[23] H.-G. Sander,[4] S. Sarkar,[36] S. Schlenstedt,[2] T. Schmidt,[16] D. Schneider,[5] D. Seckel,[9] B. Semburg,[6] S. H. Seo,[21] S. Seunarine,[3] A. Silvestri,[11] A. J. Smith,[16] M. Solarz,[12] C. Song,[5] J. E. Sopher,[13] G. M. Spiczak,[24] C. Spiering,[2] M. Stamatikos,[5,37] T. Stanev,[9] P. Steffen,[2] T. Stezelberger,[13] R. G. Stokstad,[13] M. C. Stoufer,[13] S. Stoyanov,[9] E. A. Strahler,[5] T. Straszheim,[16] K.-H. Sulanke,[2] G. W. Sullivan,[16] T. J. Sumner,[32] I. Taboada,[12] O. Tarasova,[2] A. Tepe,[6] L. Thollander,[18] S. Tilav,[9] M. Tluczykont,[2] P. A. Toale,[21] D. Turčan,[16] N. van Eijndhoven,[1] J. Vandenbroucke,[12] A. Van Overloop,[23] V. Viscomi,[21] B. Voigt,[2] W. Wagner,[21] C. Walck,[18] H. Waldmann,[2] M. Walter,[2] Y.-R. Wang,[5] C. Wendt,[5] C. H. Wiebusch,[30] G. Wikström,[18] D. R. Williams,[21] R. Wischnewski,[2] H. Wissing,[30] K. Woschnagg,[12] X. W. Xu,[26] G. Yodh,[11] S. Yoshida,[29] and J. D. Zornoza[5,38]

Received 2007 February 2; accepted 2007 March 30

[1] Department of Physics and Astronomy, Utrecht University/SRON, NL-3584 CC Utrecht, Netherlands.
[2] Deutsche Elektronen Synchrotron, D-15735 Zeuthen, Germany.
[3] Department of Physics and Astronomy, University of Canterbury, Christchurch, New Zealand.
[4] Institute of Physics, University of Mainz, D-55099 Mainz, Germany.
[5] Department of Physics, University of Wisconsin, Madison, WI 53706; brennan.hughey@icecube.wisc.edu.
[6] Department of Physics, University of Wuppertal, D-42119 Wuppertal, Germany.
[7] Institute for Advanced Study, Princeton, NJ 08540.
[8] Deceased.
[9] Bartol Research Institute and Department of Physics and Astronomy, University of Delaware, Newark, DE 19716.
[10] Vrije Universiteit Brussel, Dienst ELEM, B-1050 Brussels, Belgium.
[11] Department of Physics and Astronomy, University of California, Irvine, CA 92697.
[12] Department of Physics, University of California, Berkeley, CA 94720; itaboada@berkeley.edu.
[13] Lawrence Berkeley National Laboratory, Berkeley, CA 94720.
[14] Department of Physics, Universität Dortmund, D-44221 Dortmund, Germany.
[15] Université Libre de Bruxelles, B-1050 Brussels, Belgium.
[16] Department of Physics, University of Maryland, College Park, MD 20742.
[17] Department of Physics and Astronomy, University of Kansas, Lawrence, KS 66045.
[18] Department of Physics, Stockholm University, S-10691 Stockholm, Sweden.
[19] Division of High Energy Physics, Uppsala University, S-75121 Uppsala, Sweden.
[20] University of Mons-Hainaut, B-7000 Mons, Belgium.
[21] Department of Physics, Pennsylvania State University, University Park, PA 16802.
[22] Department of Astronomy and Astrophysics, Pennsylvania State University, University Park, PA 16802.
[23] Department of Subatomic and Radiation Physics, University of Gent, B-9000 Gent, Belgium.
[24] Department of Physics, University of Wisconsin, River Falls, WI 54022.
[25] Center for Theoretical Studies of Physical Systems, Clark-Atlanta University, Atlanta, GA 30314.
[26] Department of Physics, Southern University, Baton Rouge, LA 70813.
[27] Department of Astronomy, University of Wisconsin, Madison, WI 53706.
[28] Max-Planck-Institut für Kernphysik, D-69177 Heidelberg, Germany.
[29] Department of Physics, Chiba University, Chiba 263-8522, Japan.
[30] III Physikalisches Institut, RWTH Aachen University, D-52056 Aachen, Germany.
[31] Institut für Physik, Humboldt Universität zu Berlin, D-12489 Berlin, Germany.
[32] Blackett Laboratory, Imperial College, London SW7 2BW, UK.
[33] On leave of absence from the Università di Bari, Dipartimento di Fisica, I-70126, Bari, Italy.
[34] Affiliated with the Department of Chemistry and Biomedical Sciences, Kalmar University, S-39182 Kalmar, Sweden.
[35] Department of Physics and Astronomy, University of Alaska Anchorage, Anchorage, AK 99508.
[36] Department of Physics, University of Oxford, Oxford OX1 3NP, UK.
[37] Currently at NASA Goddard Space Flight Center, Greenbelt, MD 20771.
[38] Affiliated with IFIC (CSIC-Universitat de València), A. C. 22085, 46071 Valencia, Spain.

ABSTRACT

Using the neutrino telescope AMANDA-II, we have conducted two analyses searching for neutrino-induced cascades from gamma-ray bursts. No evidence of astrophysical neutrinos was found, and limits are presented for several models. We also present neutrino effective areas which allow the calculation of limits for any neutrino production model. The first analysis looked for a statistical excess of events within a sliding window of 1 or 100 s (for short and long burst classes, respectively) during the years 2001–2003. The resulting upper limit on the diffuse flux normalization times E^2 for the Waxman-Bahcall model at 1 PeV is 1.6×10^{-6} GeV cm^{-2} s^{-1} sr^{-1} (a factor of 120 above the theoretical prediction). For this search 90% of the neutrinos would fall in the energy range 50 TeV to 7 PeV. The second analysis looked for neutrino-induced cascades in coincidence with 73 bursts detected by BATSE in the year 2000. The resulting upper limit on the diffuse flux normalization times E^2, also at 1 PeV, is 1.5×10^{-6} GeV cm^{-2} s^{-1} sr^{-1} (a factor of 110 above the theoretical prediction) for the same energy range. The neutrino-induced cascade channel is complementary to the up-going muon channel. We comment on its advantages for searches of neutrinos from GRBs and its future use with IceCube.

Subject headings: gamma rays: bursts — neutrinos — telescopes

Online material: color figures

1. INTRODUCTION

Gamma-ray bursts (GRBs) have been proposed as one of the most plausible sources of ultra–high energy cosmic rays (Waxman 1995; Wick et al. 2004). In addition to being a major advance in neutrino astronomy, detection of high-energy neutrinos from a burst would provide corroborating evidence for the acceleration of ultra–high energy cosmic rays within GRBs.

AMANDA-II (Andrés et al. 2001), the final configuration of the Antarctic Muon and Neutrino Detector Array, is located at the South Pole. It was commissioned in the year 2000 and consists of a total of 677 optical modules. Each module contains a photomultiplier tube and supporting hardware inside a glass pressure sphere. These are arranged on 19 strings frozen into the ice, with the sensors at depths ranging from 1500 to 2000 m in a cylinder of 100 m radius. The optical modules indirectly detect neutrinos by measuring the Cerenkov light from secondary charged particles produced in neutrino-nucleon interactions. AMANDA is being integrated into the IceCube detector which is currently under construction.

Searches for neutrino-induced muons in coincidence with GRBs have been performed with the AMANDA detector for the years 1997–2003 (Achterberg et al. 2007; Stamatikos et al. 2005; Kuehn et al. 2005; Hardtke 2002; Bay 2000). Cascades, which are electromagnetic and hadronic particle showers, provide a complementary channel to muon detection (Ackermann et al. 2004). This paper presents two analyses which have searched for neutrino-induced cascade signals from GRBs. In the *rolling* search, 3 years (2001–2003) of AMANDA-II data were scanned for a clustering of signal events in time. In the *triggered* search, AMANDA-II data were analyzed for a neutrino signal in temporal coincidence with 73 bursts reported by the Burst and Transient Source Experiment (BATSE; Paciesas et al. 1999),[39] during the year 2000.

Compared to AMANDA cascade analyses, neutrino-induced muon searches have higher overall event rates because the muon's long range allows detection even if it is produced far outside the detector, while a cascade has to happen at least partially within the detector array. Muons can also use directional constraints to reduce background because their linear, tracklike shape gives them much better pointing resolution. This allows the identification of muons originating from up-going neutrinos, as these are the only known particles to propagate through the Earth.

However, these disadvantages are balanced by several arguments in favor of cascades. Since cascades are topologically distinct from AMANDA's primary background of down-going atmospheric muons, it is not necessary to use the Earth as a filter as in the case of muons. Hence, cascade analyses have full sky (4π sr) coverage, as opposed to 2π sr for muon analyses. This doubles the number of bursts that can be studied by a single detector. For the triggered analysis, this number is more than doubled, since bursts that do not have good directional localization based on satellite information can still be used in the cascade search. In addition, the energy resolution for cascades is better than that for muons because of the calorimeter-like energy deposition in the detector. For cascades produced via charged current channels which produce only showers (ν_e and ν_τ) the energy of the final state can be completely measured. Finally, on average the cascade energy is more closely correlated to that of its parent neutrino than for muons because for muons the interaction vertex is typically in an unknown place outside of the detector.

While neutrino-induced muon tracks are only caused by charged current ν_μ interactions, cascades can be produced by interactions of all three neutrino flavors. Processes producing cascade signatures include $\nu_x + N$ neutral current interactions of any neutrino flavor, $\nu_e + N$ charged current, $\bar{\nu}_e + e^-$ around 6.3 PeV (the Glashow resonance) and $\nu_\tau + N$ charged current interactions. The last case results in isolated cascade-like events when the τ decays into an electron ($\sim$18% branching ratio) or into mesons ($\sim$64% branching ratio) and the τ energy is below $\sim$100 TeV (Yao et al. 2006). The decay length of a τ with an energy of 100 TeV is approximately 5 m, so the showers produced by the neutrino interaction and by the τ decay cannot be spatially resolved by AMANDA. For neutrinos above 100 TeV, topological searches can be used to detect ν_τ (Learned & Pakvasa 1995), but in the analyses presented here we optimize for the search of isolated cascades and ignore other ν_τ event topologies. Charged current ν_μ interactions can produce cascades in addition to tracks, but this channel is ignored in these analyses in favor of cascades which are not contaminated by track-like signatures.

2. NEUTRINOS FROM GAMMA-RAY BURSTS

It is believed that gamma rays produced by GRBs originate from electrons accelerated in internal shock waves associated with relativistic jets (with a bulk Lorentz boost Γ of 100–1000) (Mezsáros & Rees 1994; Paczynski & Xu 1994). These gamma rays have energies ranging from 10 keV to 10 MeV or more. The gamma-ray spectrum can be generically described as a broken

[39] See http://www.batse.msfc.nasa.gov/batse/grb/catalog/.

power law, with a softer spectrum above a break energy, which is typically 30 keV–1 MeV. Gamma-ray bursts can last anywhere from a few milliseconds to around 1000 s. The distribution (as observed by BATSE) of durations is bimodal. For the purposes of these analyses, we define as *short* bursts those that last less than 2 s and as *long* bursts those that last longer than 2 s (Paciesas et al. 1999). Other types of bursts have been proposed, but the searches presented here do not apply to these classes. Reviews of the observational and theoretical status of gamma-ray bursts may be found in Zhang & Meszáros (2004) and Piran (2005).

If protons and/or nuclei are also accelerated in the jets, then high energy (TeV–PeV) neutrinos are produced via the process (Waxman & Bahcall 1997):

$$p + \gamma \rightarrow \Delta^+ \rightarrow \pi^+[+n] \rightarrow \nu_\mu + \mu^+ \rightarrow \nu_\mu + e^+ + \bar{\nu}_\mu + \nu_e. \quad (1)$$

The kinematics of this reaction are such that the average energy of each neutrino is approximately the same, so the neutrino flavor ratio $\nu_e : \nu_\mu : \nu_\tau$ is $1:2:0$ at the source. Taking into account neutrino oscillations, the flavor ratio observed at Earth is 1:1:1 (Athar et al. 2006). However, Kashti & Waxman (2005) point out that at energies greater than $\sim$1 PeV, the μ^+ in equation (1) loses energy through synchrotron radiation before decaying. This effect changes the source neutrino flavor ratio from $1:2:0$ to $0:1:0$ as energy increases, leading to a ratio at Earth of 1:1.8:1.8 at high energies for the Waxman-Bahcall neutrino spectrum.

Even at energies where the flavor ratio is 1:1:1, the $\nu:\overline{\nu}$ ratio is not 1:1. This is because neutrinos are produced via the $p\gamma$ interaction. At the source the neutrino flavor ratio (excluding antineutrinos) is 1:1:0 and the antineutrino flavor ratio is 0:1:0. After taking into account preferred values of mixing angles (Maltoni et al. 2004) for neutrino oscillations the flux ratios at Earth are 0.8:0.6:0.6 and 0.2:0.4:0.4 for neutrinos and antineutrinos respectively. The $\nu:\overline{\nu}$ flux ratio is relevant in the calculation of the total number of expected events by the detector.

TeV–PeV neutrinos are expected to be simultaneous with prompt gamma-ray emission. The neutrino spectrum is described by a broken power law. For both searches presented in this paper we use the Waxman & Bahcall (1997) broken power-law spectrum as a reference hypothesis and to optimize our data selection criteria. This spectrum is

$$\frac{d\Phi_\nu}{dE} = A \begin{cases} E^{-1}/E_b, & E < E_b \\ E^{-2}, & E_b < E < E_\pi \\ E^{-4}E_\pi^2, & E > E_\pi \end{cases}, \quad (2)$$

where A is the flux normalization, E_b is the break energy corresponding to the break in the parent photon spectrum and E_π is the energy break due to pion energy losses. Following Waxman & Bahcall (1997) and Waxman (2003) we set $E_b = 100$ TeV, $E_\pi = 10$ PeV, and $A = 1.3 \times 10^{-8}$ GeV cm^{-2} s^{-1} sr^{-1} at the Earth for all neutrino flavors combined. In reality, each GRB is unique and the spectral shape and normalization of individual GRBs may vary significantly from this assumed "typical" spectrum (Guetta et al. 2004; Stamatikos et al. 2005). The rolling search, however, is conducted independent of external triggers. This frees the search from detector selection effects introduced by the gamma-ray satellites, but makes optimizing on an averaged spectrum the only viable option. For the triggered analysis we have chosen to optimize the selection criteria with the mean spectrum as well. Also, selection criteria optimization is not strongly dependent on the exact shape of the signal spectrum.

Newer models update the Waxman-Bahcall model with current knowledge. Murase & Nagataki (2006) have performed a detailed simulation of neutrino production in internal shocks in GRBs. The authors use several models for the redshift distribution of GRBs, e.g., one assumption is that the (long duration) GRB rate follows the star formation rate. They vary several parameters, such as spectral hardness, to reflect current unknowns. In this paper we present limits on the Murase-Nagataki model. Guetta et al. (2004) have improved on Waxman-Bahcall with a phenomenological approach. They have used information specific to bursts reported by the BATSE detector on the Compton Gamma Ray Observatory satellite to predict neutrino fluences on a burst by burst basis. However, Guetta et al. (2004) do not provide neutrino fluences for all 73 bursts used in the triggered analysis.

Many theoretical predictions also account for neutrino emission following different spectral shapes both before and after the burst. These include precursor neutrinos coming from the GRB jet while it is still within the progenitor (Meszáros & Waxman 2001; Razzaque et al. 2003a) and afterglow neutrinos resulting from interactions with the interstellar matter encountered by the relativistic GRB jet (Waxman & Bahcall 2000). The analyses presented in this paper, however, are optimized for the Waxman-Bahcall prompt neutrino emission spectrum only.

3. RECONSTRUCTION AND SIMULATION

In both the rolling and triggered analyses, events were reconstructed with iterative maximum likelihood reconstructions using both cascade and muon hypotheses, the latter to reject background. The cascade hypothesis reconstruction provides a vertex, while the muon hypothesis reconstruction provides a vertex as well as zenith and azimuth angles. In addition to these, the triggered analysis uses a cascade hypothesis energy reconstruction. For simulated signals we obtain a cascade vertex resolution of about 6 m horizontally and slightly better vertically. The cascade energy resolution, defined as the rms of the $\log_{10}(E_{\rm true}/E_{\rm reco})$ distribution is approximately equal to 0.15, where $E_{\rm true}$ is the actual energy and $E_{\rm reco}$ is the reconstructed energy. For simulated downgoing muons the zenith resolution is approximately 5°. The downgoing muon angular resolution is worse than for other analyses because a simpler muon reconstruction is sufficient for muon rejection. Cascade and muon reconstruction methods are described in Kowalski (2004), Taboada (2002), and Ahrens et al. (2003a, 2004). Cascade reconstruction algorithms have been tested using artificial signals created by LEDs and lasers deployed in different locations of the array. These sources produce photonic signatures similar to cascades (Kowalski 2004; Taboada 2002). These tests give us confidence that we understand the detector sensitivity to neutrino-induced cascades.

Both analyses used ANIS (Gazizov & Kowalski 2005) for signal simulation. All three neutrino flavors were simulated with an E^{-1} signal spectrum, which was then reweighted to a broken power law. Muon background (including multiple muons) was simulated using CORSIKA (Heck 1998). Propagation of muons through ice was simulated using MMC (Chirkin & Rhode 2001) and detector response was simulated using AMASIM (Hundertmark 1998). For both analyses the background is measured experimentally (see §§ 4 and 5). However, background simulation was used to verify our understanding of the detector by comparing the distribution of selection parameters in experimental data and simulation.

4. ROLLING ANALYSIS

While satellites detect many GRBs each year, it is clear that the photonic signatures of many bursts are missed by gamma-ray satellites. This was especially true during the years 2001–2003,

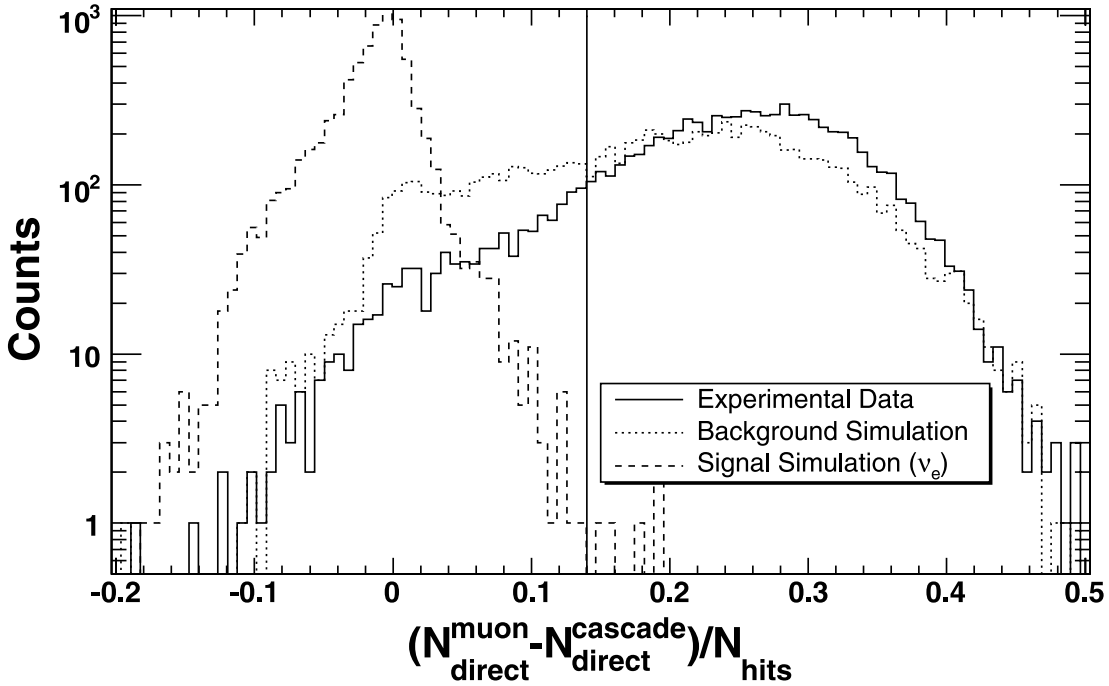

FIG. 1.—Cut variable $(N_{\rm dir}^{\rm muon} - N_{\rm dir}^{\rm cascade})/N_{\rm hits}$. Values above 0.14 are removed. $N_{\rm dir}$ is the number of hits for which there has been no scattering of the photons in the ice.

the timeframe during which the rolling analysis was conducted, which was after BATSE ceased operations in 2000 and before *Swift* launched in 2004. Rather than rely on satellite coincidence, the rolling analysis searches for a statistical excess of events in close temporal coincidence by sliding a time window of fixed duration over the entire data set. Since no satellite triggers were used, this analysis could also potentially identify neutrino signals from previously unknown photon-dark transients and hence is not limited exclusively to GRBs. Furthermore, it is still an unresolved question if neutrinos arrive in coincidence with the prompt photons or if there is a time offset. In either case, the rolling analysis would be sensitive to GRB neutrinos.

Since BATSE results demonstrate that the distribution of GRBs is bimodal (Paciesas et al. 1999), two separate time windows were used, with durations of 1 and 100 s. Although these choices do truncate the signal from some longer bursts (assuming the neutrino burst duration is identical to the gamma burst duration), they are the most appropriate. By studying an ensemble of real light curves from the BATSE 4B catalog, we conclude that the gain in signal efficiency for a small percentage of the bursts from widening the time windows would not justify the increase in average background rate for all windows. The numbers are kept at round values because the optimization process is not precise enough to distinguish optimal durations to within a few percent.

Without an external trigger, the most efficient search for a clustering of events is conducted by starting a new window at the time of each event that remains after cuts and counting the number of additional events in the following 1 or 100 s.

4.1. *Data Selection*

Data used in the rolling analysis come from the 2001, 2002, and 2003 AMANDA-II data sets. To ensure stability of the data, the austral summer periods from late October to mid February when the South Pole station was open were omitted. Significant work was being done on the detector and the surrounding area at this time, which could potentially interfere with the long term stability of the data sample during that period. Bad files were removed from the analysis applying the same standards as AMANDA point source searches (Ackermann et al. 2005). Runs less than 5000 s and files with a large number of gaps (due to unstable periods in the data) were also excluded. Deadtime percentages were 21.3% for 2001, 15.0% for 2002, and 15.3% for 2003. Adjusting for deadtime, the livetimes for the data sets used in this analysis were 183.4 days for 2001, 193.8 days for 2002, and 185.2 days for 2003, yielding a total livetime of 562.4 days.

Since there are no spatial or temporal constraints in this analysis, background rejection is extremely important. The first step is the application of a high energy filter, which cuts out events with fewer than 160 hits[40] or events where fewer than 72% of optical modules had two or more hits. This was followed by a process referred to as "flare checking," which is designed to remove nonphysical events resulting from short-duration detector instabilities or detector malfunction (Pohl 2004).

To further reduce the background, a loose cut was made on the variable $N_{\rm direct}$, which is the number of hits for which there has been no scattering of the photons in the ice. For the 2001 data set, the exact definition used for this cut was $N_{\rm direct}^{\rm muon}/N_{\rm hits}$, where $N_{\rm direct}^{\rm muon}$ is the number of direct hits using the iterative muon fit and $N_{\rm hits}$ is the total number of hits. The $N_{\rm direct}$ cut is useful because cascade-like events will generally have fewer direct hits under the muon hypothesis than good muon tracks would. Dividing by $N_{\rm hits}$ removes the tail of high-energy events, which have a large value of $N_{\rm direct}^{\rm muon}$, simply because of the large number of total hits in the event. After the 2001 data had been analyzed, a somewhat improved cut, defined as $(N_{\rm direct}^{\rm muon} - N_{\rm direct}^{\rm cascade})/N_{\rm hits}$, was developed and applied to the 2002 and 2003 data sets, but was not retroactively applied to the 2001 data because this sample was previously unblinded and we did not wish to introduce trials factor penalties by altering the selection criteria. As the agreement between data and simulation is imperfect in this variable (see Fig. 1) cutting too close to the signal peak would introduce large systematic

[40] A "hit" occurs each time an optical module's voltage rises above a preset threshold, generally resulting from the detection of a photon.

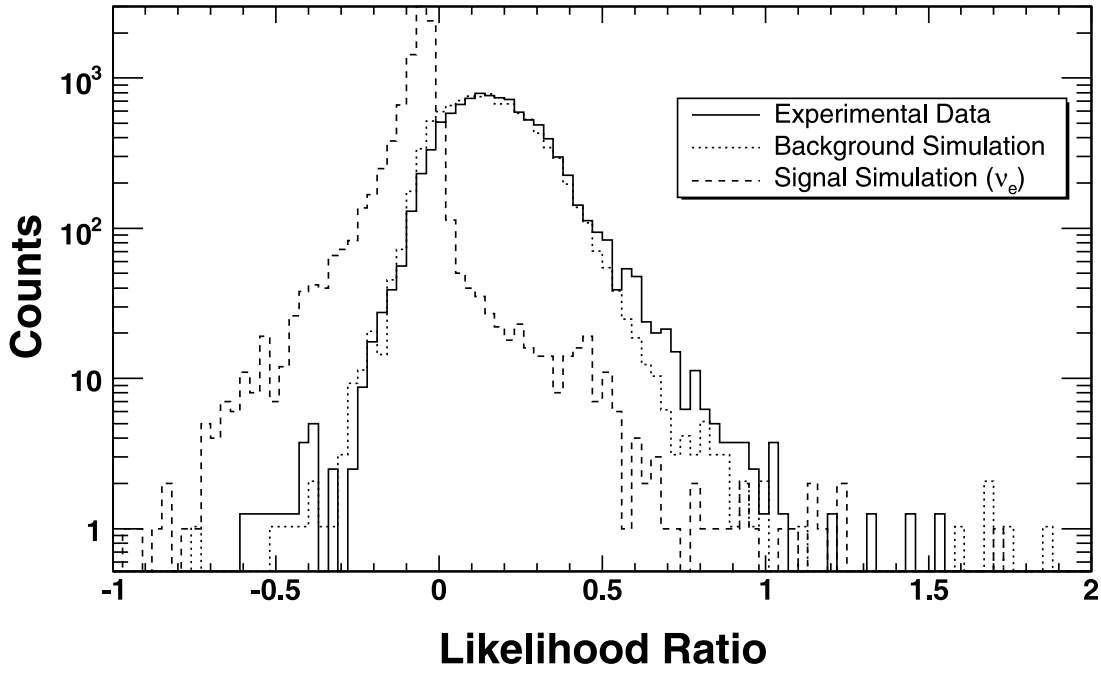

FIG. 2.—Likelihood ratio compares the likelihood of a given event being a muon to the likelihood of it being a cascade. This variable is shown as a representative example of the six variables used in the SVM cut.

uncertainties. Therefore, this variable is not included in the final cut optimization where its position cannot be controlled, but rather used as a conservative initial cut.

The final step in data reduction is a six variable support vector machine (SVM) trained with the program SVM$^{\text{light}}$ (Joachims 1999). An SVM uses a mathematical kernel function to find optimal cuts in a multidimensional variable space. The user is allowed to adjust a variable called the "cost factor," by which tighter or looser cuts can be obtained. Five days of data were used from each year as background to train the SVM, while ANIS simulation was used as signal. Cuts were finalized using only this subsample, which was not used for the final analysis. This was done because of the standards of blindness applied to all AMANDA analyses. These require that all analysis criteria are decided before looking at the data in order to avoid artificially increasing the significance of an observation through biased cut selection. The six variables used in the SVM are a combination of topological cuts, which keep cascade-like signatures and reject muon signatures, and energy-related cuts, which keep events that have properties consistent with higher energies. These variables are as follows:

1. Likelihood ratio between the muon and cascade iterative likelihood reconstructions: this variable provides a useful means of distinguishing between events with cascade and tracklike properties. This variable is shown in Figure 2. As with the five other variables used in the SVM, good agreement is observed between data and background simulation.

2. Percentage of optical modules with eight or more hits: this is influenced by both the energy and type of event, as both high energy events and events producing a significant shower of particles will tend to produce multiple hits in each optical module.

3. Length along the track spanned by the direct hits: this is the length over which the direct hits are distributed. This track length will naturally be shorter on average for the more spherically shaped cascades.

4. $N_{\text{late}}^{\text{cascade}} - N_{\text{late}}^{\text{muon}}$: this variable compares the number of hits that arrive more than 150 ns late relative to the fit using the cascade and muon hypotheses.

5. $N_{\text{hits}}/N_{\text{OM}}$: this variable gives the average number of hits per optical module with hits. Like the percentage of modules with eight or more hits, this variable selects high-energy cascades, which produce on average more hits per module than other events.

6. Velocity of the line fit: the line fit is a relatively fast algorithm that fits a line with velocity v to each event (Ahrens et al. 2004). Cascade-like events will yield smaller velocities than muon events, which should ideally have line speeds close to the speed of light.

The output of the SVM is displayed in Figure 3, showing good agreement between data and simulated background.

4.2. *Optimization*

The primary observable in the rolling analysis is N_{large}, the largest number of events occurring in any search window during the 3 year period. Based on the distribution of predicted neutrino fluences, detection of a single burst with exceptionally high neutrino fluence is statistically more probable than detection of events from multiple bursts. The analysis is optimized for discovery as described in Hill et al. (2005) selecting the final cut (i.e., SVM cost factor) to minimize the source neutrino flux required to produce a 5 σ observation with better than 90% probability. The final sensitivity, however, is only $\sim$7% above the value obtained for sensitivity-optimized cuts. Short and long time windows were optimized independently. It was assumed that background events were distributed according to Poissonian statistics. The data are quite consistent with this assertion (see Fig. 4). Background rates are not identical over the entire year, since the down-going muon rate varies with atmospheric temperature. Therefore, rather than assuming a single average Poissonian background rate, the background was characterized by using different mean background rates for several periods during each year.

With the chosen selection criteria, a cluster of five events in a 1 s window or seven events in a 100 s window would be required for a 5 σ detection. Passing rates for the various cut stages in this

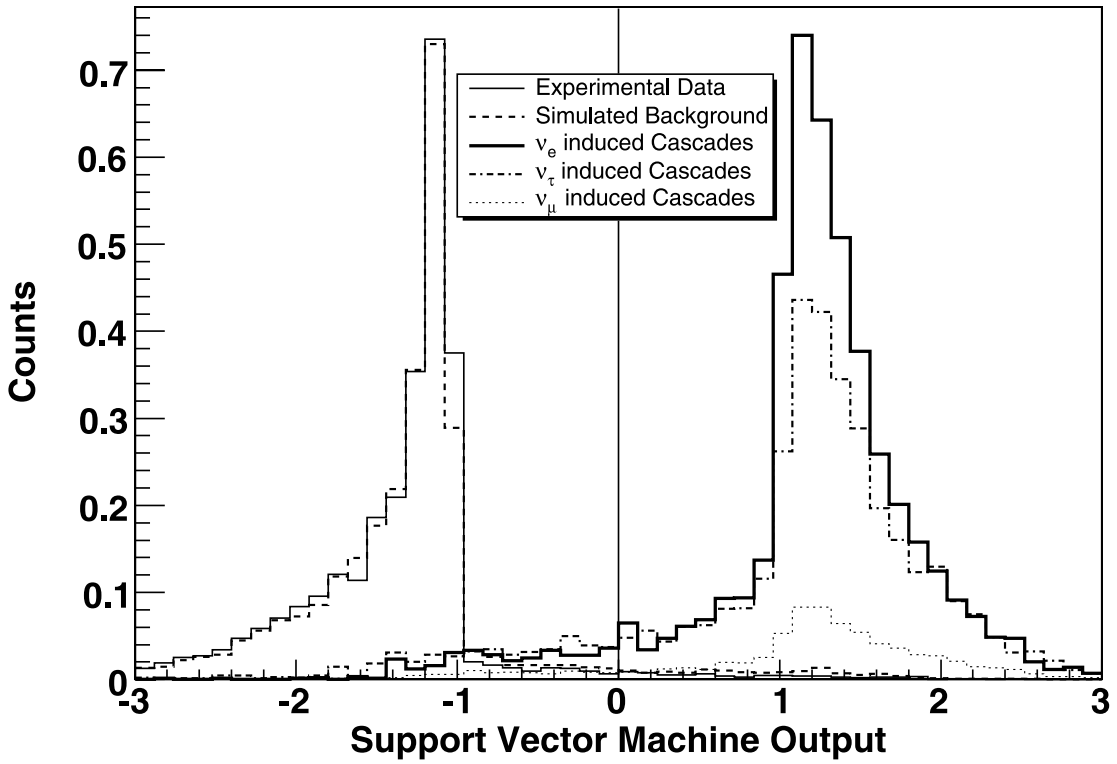

FIG. 3.—SVM output for experimental data, simulated background and simulated signal resulting from the three neutrino flavors. Values above zero are considered signal, while those below zero are considered background and rejected. Muon neutrino signal simulation corresponds to neutral current interactions.

analysis are shown in Table 1. We now turn to a discussion of the previously mentioned triggered analysis.

5. TRIGGERED ANALYSIS

AMANDA-II began routine operation on 2000 February 13. The last BATSE burst was reported 2000 May 26. We have used this period of time for a coincident search of neutrino-induced cascades and GRBs.

The Large Area Detectors (LADs) of BATSE had four energy channels: channel 1 (20–50 keV), channel 2 (50–100 keV), channel 3 (100–300 keV), and channel 4 (>300 keV). After 2000 February 14, the trigger condition for BATSE was a 5.5 σ

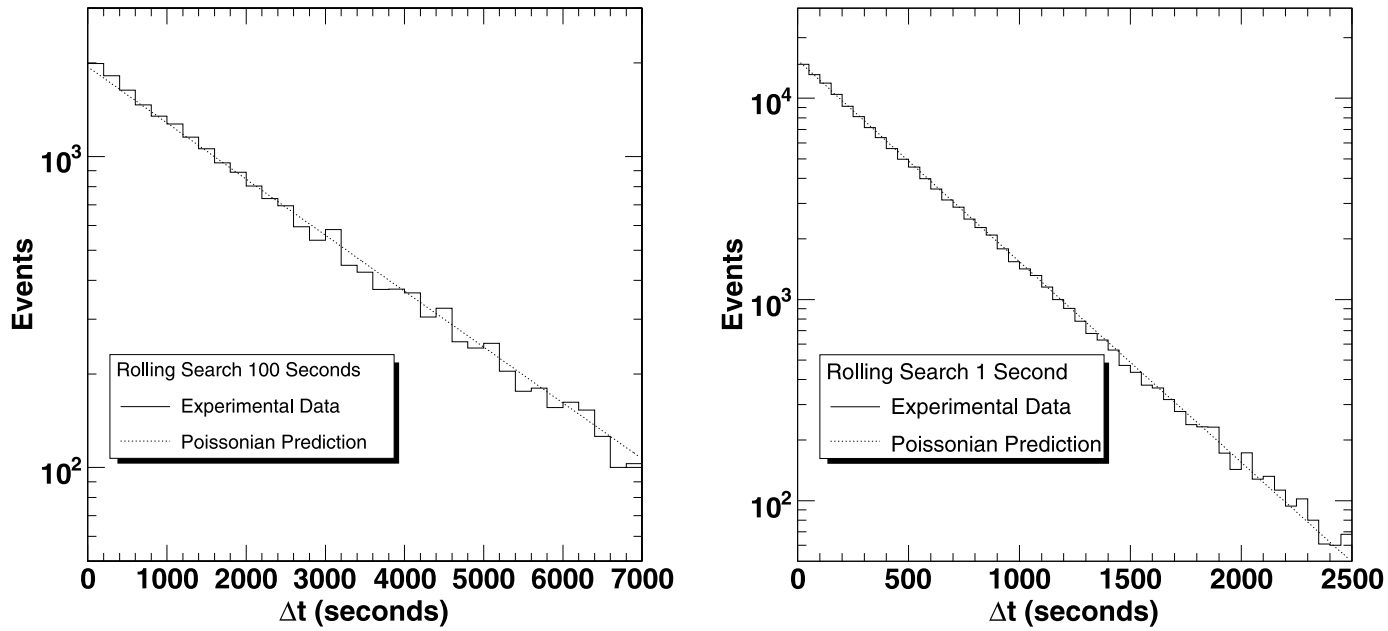

FIG. 4.—Time difference Δt between surviving events for both the 100 s (*left*) and 1 s (*right*) searches. The solid line shows experimental data for all 3 years in which the analysis was conducted. The dotted line shows the theoretical prediction, modeling the background with a Poisson distribution and dividing each year into five periods with unique Poissonian average rates. Because the two time windows were optimized independently, these curves correspond to different average event rates: 1 event per 2404 s for the long-window search (*left*) and 1 event per 427 s for the short-window search (*right*).

TABLE 1

PASSING RATES FOR EXPERIMENTAL DATA AND SIMULATED WAXMAN-BAHCALL SPECTRUM, $\nu_e + \bar{\nu}_e$

Parameter	Experimental Data (%)	$\nu_e + \bar{\nu}_e$ (%)
Initial	100	100
Filter	0.80	62
$N_{\rm dir}$ cut	0.10	62
SVM short window search	0.0027	58
SVM long window search	0.00040	43

TABLE 2

SIMULATED $\nu_e + \bar{\nu}_e$ PASSING RATES FOLLOWING A WAXMAN-BAHCALL SPECTRUM AND *Off-Time* WINDOW PASSING RATES FOR THE TRIGGERED ANALYSIS

Parameter	Off-Time (%)	$\nu_e + \bar{\nu}_e$ (%)
Initial	100	100
Filter	0.91	67
$L_{\rm mpe} < 6.9$	0.05	35
$E_c > 40$ TeV	4×10^{-6}	25

deviation from background on the sum of channels 3 and 4 for three different timescales: 64, 256, and 1024 ms. Except for one burst, GRB 000213, all bursts used in this paper were triggered as described. For GRB 000213 triggering was done with channel 3 only.

Since the GRB start time, S_{90}, and duration, T_{90}, are well known, the separation of neutrino-induced cascade signals from the down-going muon background is simplified. We use three selection criteria based on the two reconstruction hypotheses to discard the down-going muon background and keep the neutrino-induced cascade signal.

These criteria are

1. Reconstructed muon zenith angle, θ_μ: this is the reconstructed zenith angle of the muon hypothesis. We reject events that are consistent with down-going muons, corresponding to $0^\circ < \theta_\mu < 90^\circ$. For simulated cascade signals there is no correlation between neutrino zenith angle and the reconstructed muon zenith angle.
2. Cascade reconstruction reduced likelihood, $L_{\rm mpe}$: this is the likelihood parameter (or reduced likelihood) of the multiple photoelectron cascade-vertex reconstruction. Smaller values correspond to events that match the cascade hypothesis and large values correspond to events that are not cascade-like.
3. Reconstructed cascade energy, E_c: this is the energy of the cascade hypothesis. Because the energy spectrum of the Waxman-Bahcall model is hard, the selection criterion $E_c > E_{\rm cut}$ is good at separating signal from background.

A total of $\sim$7800 s per burst were studied. A period of 600 s, the *on-time* window, centered at the start time of the GRB, was initially set aside in accordance with our blind analysis procedures. The hour just before and the hour just after the on-time window, called the *off-time* windows, are also studied. We optimize the selection criteria using the off-time windows and signal simulation. Thus the background is experimentally measured. We only examined the fraction of the on-time window corresponding to the duration of each burst. Keeping the rest of the on-time window blind allows for other future searches, e.g., precursor neutrinos. We use T_{90} as the duration of the burst, where the time window starts when the GRB has emitted 5% of its total fluence and ends when 95% have been emitted. As a precaution against possible uncertainties in the timing of the bursts we expanded T_{90} by 1 s on both sides and by the uncertainty of the duration U_{90}. We call 1 s + T_{90} + U_{90} + 1 s the *signal* window. The values for U_{90} were obtained from the BATSE catalog and the typical value is 1 s.

5.1. *Data Selection*

We applied the selection criteria in two steps, a filter and the final selection. The filter rejects down-going muons with $\theta_\mu > 70^\circ$, and keeps events that are cascade-like, $L_{\rm mpe} < 7.8$. The filter was selected so as to maximize signal efficiency while reducing the background. The procedure for establishing the final set of selection criteria is explained in § 5.2. Table 2 shows the passing rate of the filter.

We determined the detector stability using the off-time window experimental data after the filter was applied. Only GRBs for which the detector is found to be stable in the off-time windows were used for the neutrino search.

To establish the stability of the detector, first, bad observation runs were removed from the year 2000 data set following the same collaboration-agreed scheme used for the rolling analysis. For GRB 000508a, AMANDA fails this test. We also checked that there are no data gaps, i.e., times the detector was off within the T_{90} of the burst. For GRB 000330a there are gaps in AMANDA data. We also checked the stability of the detector by studying the off-time windows. Two quantities were examined, the number of events/10 s that pass the filter as a function of time and the frequency distribution of events/10 s after applying the filter. Figure 5 shows the distribution of event rates around a good burst. Visual inspection of the events/10 s versus time showed a problem with AMANDA data corresponding to burst GRB 000331a. Several AMANDA strings failed to collect/report data for periods of time on the order of 10–100 s. For this reason, GRB 000331a was excluded from this analysis. We have also looked at the plots of time difference between events to check for possible detector problems. No new problems were found. Finally, we also exclude GRB 000217a and GRB 000225 from the list of bursts because AMANDA was not operational for these two bursts.

After all these criteria are used we find 73 BATSE bursts for which the detector is behaving stably. Of these bursts, 53 are long bursts ($T_{90} > 2$ s) and 20 are short bursts ($T_{90} < 2$ s). In the BATSE catalog (Paciesas et al. 1999) T_{90} values were not available for 13 bursts. The lack of T_{90} may be caused by gaps in the BATSE data not being treated properly by automatic procedures. In this case the light curves for the bursts without T_{90} were obtained from BATSE's Web site. The comments in the web page were also studied. Based on visual inspection of the light curves and the comments, conservative, i.e., large, values for burst duration were chosen. For 12 of the bursts with missing T_{90} we examined the light curves for the combined channels 1–4. For burst GRB 000517 we used the light curve for the combined channels 1–3, since channel 4 was missing. Table 3 summarizes the characteristics of the 78 bursts (73 used in this analysis) reported by BATSE between 2000 February 13 and May 26.

5.2. *Optimization*

The selection criteria were optimized on the off-time windows for discovery in a procedure similar to that of the rolling analysis but with the difference that we optimize two selection criteria simultaneously. The final selection criteria are $L_{\rm mpe} < 6.9$ and $E_c > 40$ TeV. Figure 6 shows the $L_{\rm mpe}$ and E_c distribution after

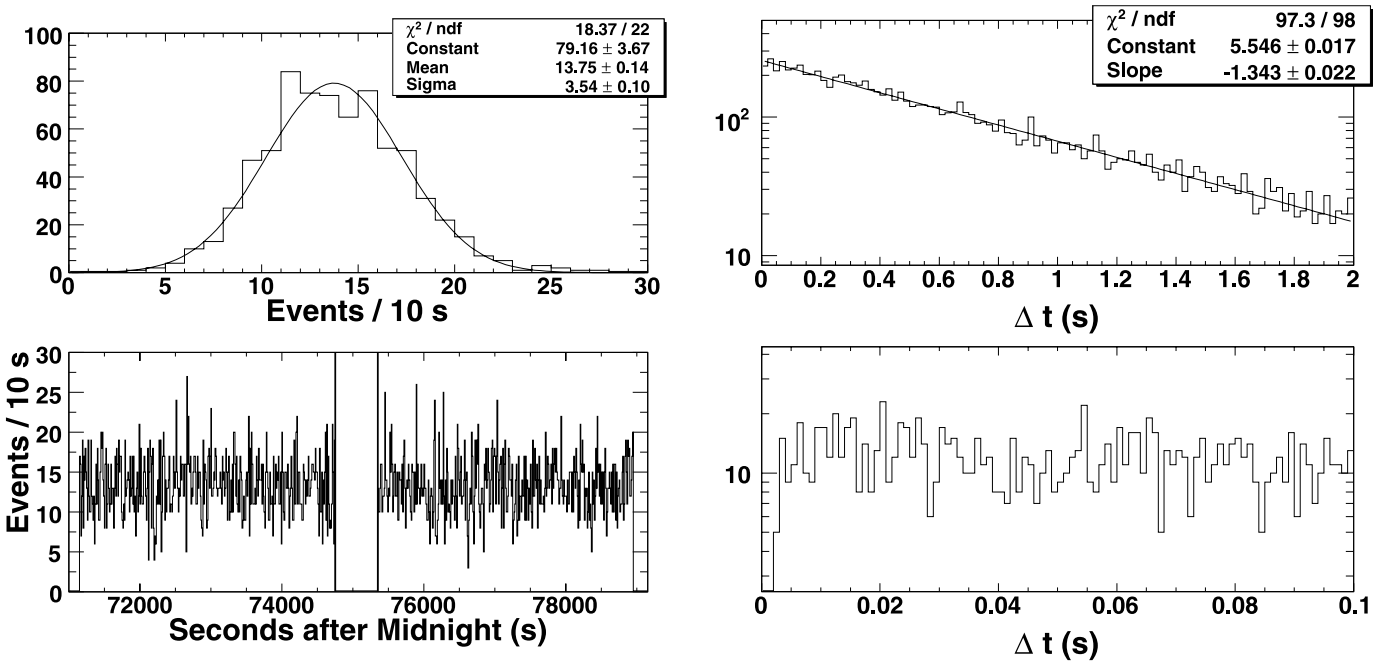

FIG. 5.— *Top left*: Distributiondistribution of frequency of events/10 s after the filter has been applied for GRB 000312b. *Bottom left*: Events/10 s vs. time. The gap in the middle of the bottom left panel corresponds to the on-time window. The top right panel shows the distribution of time difference, Δt, between consecutive events in the range 0–2 s. The bottom right panel is the same as the top right, but in the range 0–0.1 s. The gap observed near $\Delta t = 0$ is due to DAQ dead time.

the filter has been applied for the data in the *signal* window, along with simulated background and simulated neutrino signal. After all selection criteria are applied, one event remains in the 73 burst combined off-time windows. This is equivalent to an expected background of $n_b = 0.0054^{+0.013}_{-0.005}$ (stat) in the 73 burst combined *on-time* window. Passing rates for the various cut stages in this analysis are shown in Table 2. Three or more on-time, on-source events would be required for a 5 σ detection.

The total *signal* window is 2851.44 s corresponding to 2591.61 s for T_{90}, 113.83 s for the sum of the uncertainty on T_{90} and 146 s for the padding of the on-time window. The total *off-time* window is 529329 s. For the specific set of runs used in this search the AMANDA-II dead time is 17.8%.

6. SYSTEMATIC UNCERTAINTIES

Multiple effects have to be considered when estimating the systematic uncertainties: properties of the ice, detector effects, neutrino-matter cross-sections, etc. We have used signal simulations to estimate the uncertainties and artificial light sources to verify that the detector is sensitive to cascade-like signals (Kowalski 2004; Taboada 2002).

The actual optical properties of ice at the South Pole are known with a reasonably high degree of precision (Ackermann et al. 2006), but this knowledge is not fully incorporated into the signal simulation software that was available for this paper. The IceCube collaboration is working on improved simulation software so that better optical ice models are available for future analyses.

To estimate the systematic uncertainty due to the optical properties of the ice we have performed signal simulations supposing a Waxman-Bahcall spectrum using the most and least transparent ice that has been measured at AMANDA depths. In the triggered analysis we find 30% more signal events than with average optical properties for the clearest ice and we find 65% fewer events than with average optical properties for the least transparent ice. In the rolling analysis we find 50% more signal events in the clearest ice and 50% fewer events in the least transparent ice. It should be noted that these systematic uncertainties are not rms ranges, instead they are extreme values. We will suppose that systematic uncertainties have a flat distribution between the extrema found. The equivalent rms values are $^{+9}_{-19}$ % for the triggered analysis and $\pm 14\%$ for the rolling analysis. The systematic uncertainties due to ice properties in this paper are larger than in our previous publications on neutrino-induced cascades (Ahrens et al. 2003a; Ackermann et al. 2004). This is because for the previous publications an E^{-2} spectrum was assumed. For hard spectra such as Waxman-Bahcall (see eq. [2]), the uncertainty due to optical properties of ice is larger. In addition, we use different selection criteria.

We followed a similar procedure for estimating the effect of the uncertainty in the absolute efficiency of the optical modules. A 10% uncertainty in the absolute efficiency results in a change of 3% in the number of signal events in the triggered analysis and a 5% change in the rolling analysis. Similarly, a 5% uncertainty in the neutrino-matter cross section (Gandhi et al. 1999) results in a 4% change in the number of signal events. Other effects like OM prepulsing (Ahrens et al. 2003a), electronic crosstalk, and differences between data and simulation make negligible contributions to the systematic uncertainties.

In the case of the rolling analysis, there is also a $\pm 20\%$ percent uncertainty in the final limit resulting from the uncertainty in the burst-by-burst spread of neutrino fluxes. This uncertainty results from several factors, primarily variations in the distribution of events depending on what model parameterizations are used and uncertainty in the fit applied to the data. This procedure is explained in more detail in § 7.1.

We thus find that the simulation of optical properties of ice is the single most important contribution to the systematic uncertainties. Adding in quadrature the signal systematic uncertainties results in a global signal uncertainty of $^{+31}_{-65}$ % for the triggered analysis and $\pm 54\%$ for the rolling analysis.

7. RESULTS

For both the rolling and triggered analysis we do not find evidence of neutrino-induced cascades from gamma-ray bursts.

TABLE 3
List of Bursts Used for the Triggered Analysis

BATSE ID	Burst	T_{90} (s)	R.A. (J2000.0) (deg)	Decl. (J2000.0) (deg)
7988.....	GRB 000213	0.41	4.80	225.14
7989.....	GRB 000217a	30.57	36.51	126.25
7990.....	GRB 000217b	n/a[a]	−56.97	337.12[b]
7991.....	GRB 000219	1.00	84.14	116.37[c]
7992.....	GRB 000220	2.45	65.95	129.86
7994.....	GRB 000221	26.18	77.70	136.20
7995.....	GRB 000222	0.61	60.60	141.82
7997.....	GRB 000225	16.70	0.53	215.99[a]
7998.....	GRB 000226a	10.24	29.82	197.28
7999.....	GRB 000226b	0.53	16.89	74.58
8001.....	GRB 000227	75.14	−7.49	184.37
8002.....	GRB 000228	15.00	65.16	99.50[c]
8004.....	GRB 000229	32.51	47.87	81.33
8005.....	GRB 000301	25.00	72.68	120.17[c]
8008.....	GRB 000302a	22.66	54.28	147.47
8009.....	GRB 000302b	14.34	30.66	196.18
8012.....	GRB 000303	17.66	62.05	91.46
8018.....	GRB 000306a	0.13	−10.17	206.83
8019.....	GRB 000306b	51.20	40.92	68.39
8022.....	GRB 000307	22.53	6.80	200.18
8026.....	GRB 000310a	327.30	−10.86	234.59
8027.....	GRB 000310b	1.54	−1.46	106.10
8030.....	GRB 000312a	23.87	37.92	83.64
8031.....	GRB 000312b	45.00	11.04	200.09[c]
8033.....	GRB 000313a	0.13	−19.37	343.91[c]
8035.....	GRB 000313b	0.77	10.25	319.57
8036.....	GRB 000314	110.85	50.66	167.77
8039.....	GRB 000317	83.52	32.66	136.70
8041.....	GRB 000319	0.08	−13.86	275.00
8045.....	GRB 000320	44.16	4.44	199.27
8047.....	GRB 000321	0.89	36.39	153.04
8049.....	GRB 000323	72.45	48.08	126.91
8050.....	GRB 000324	3.90	−24.04	319.19
8053.....	GRB 000326a	1.92	−26.36	24.96
8054.....	GRB 000326b	21.25	−63.47	330.45
8056.....	GRB 000330a	26.00	32.00	74.84[b]
8057.....	GRB 000330b	0.40	39.26	110.80[c]
8058.....	GRB 000331a	25.00	−15.02	271.73[b]
8059.....	GRB 000331b	78.66	−46.29	290.09
8061.....	GRB 000331c	26.94	59.77	132.44
8062.....	GRB 000401	133.44	80.60	112.87
8063.....	GRB 000402	106.62	6.65	78.59
8064.....	GRB 000403	148.22	24.69	166.48
8066.....	GRB 000407	28.93	−70.06	291.50
8068.....	GRB 000408a	0.62	−71.85	319.61
8069.....	GRB 000408b	4.78	67.22	146.61
8071.....	GRB 000409	41.34	80.82	112.91
8072.....	GRB 000410	0.35	−12.48	327.83
8073.....	GRB 000412	33.02	−59.78	307.21
8074.....	GRB 000415a	11.00	68.27	132.37[c]
8075.....	GRB 000415b	20.80	69.42	144.65
8076.....	GRB 000415c	0.22	−29.98	309.64
8077.....	GRB 000417	1.66	2.93	357.46
8079.....	GRB 000418	2.29	76.15	135.19
8080.....	GRB 000420a	140.00	−44.66	267.84[c]
8081.....	GRB 000420b	46.00	−14.59	238.81[c]
8082.....	GRB 000420c	10.11	−63.01	332.47
8084.....	GRB 000421	82.18	16.98	240.68
8085.....	GRB 000424a	3.58	71.80	107.62
8086.....	GRB 000424b	18.43	53.98	162.56
8087.....	GRB 000429	164.35	−4.81	216.02
8089.....	GRB 000502	0.12	−46.68	339.87
8097.....	GRB 000508a	1.00	3.78	326.62[b]
8098.....	GRB 000508b	136.19	−20.38	0.51
8099.....	GRB 000508c	15.49	2.39	204.79
8100.....	GRB 000509	20.00	−39.27	358.61[c]
8101.....	GRB 000511a	115.01	−36.11	8.02
8102.....	GRB 000511b	38.98	−8.70	30.83
8104.....	GRB 000513a	0.38	−45.11	350.24
8105.....	GRB 000513b	11.33	−12.01	260.19
8109.....	GRB 000517	51.00	76.74	137.86[c]
8110.....	GRB 000518	10.30	53.91	153.22
8111.....	GRB 000519	14.59	3.33	78.40
8112.....	GRB 000520	14.98	−0.31	5.64
8113.....	GRB 000521	2.00	−6.25	104.25[c,d]
8116.....	GRB 000524	49.98	−41.36	252.93
8120.....	GRB 000525	1.41	−39.44	355.92
8121.....	GRB 000526	36.86	−10.32	353.05

[a] No T_{90} in catalog.
[b] Burst not used for triggered analysis.
[c] Duration selected by visual inspection of the light curves.
[d] We classify this burst as short.

We derive limits on the total diffuse neutrino flux due to all GRBs using the Feldman & Cousins (1998) unified procedure. We include systematic uncertainties following Conrad et al. (2002) and Hill (2003). Our limits depend on the modeling of the distribution with redshift of gamma-ray bursts (Jakobsson et al. 2005). For the triggered analysis the models use burst distributions that follow the experimental selection effects of BATSE. The rolling analysis is not constrained by these selection effects and thus long duration bursts should be modeled as following the star formation rate. In practice, however, we use the same distribution for both analyses because the difference between the two options is extremely small. This is probably because only bursts with relatively high fluence contribute significantly to the neutrino flux.

We present model rejection factors (MRF)[41] (Hill & Rawlins 2003) for Waxman & Bahcall (1997), Razzaque et al. (2003b), Meszáros & Waxman (2001), and Murase & Nagataki (2006) model A. For the Waxman-Bahcall model we assume 1:1:1 flavor flux ratio, $p\gamma$ neutrino generation, 666 bursts yr^{-1}, and a flux normalization[42] of $A_{\nu_e+\nu_\mu+\nu_\tau} = 1.3\times10^{-8}$ GeV cm^{-2} s^{-1} sr^{-1}. We ignore the transition from 1 : 1 : 1 flux ratio to 1:1.8:1.8 with increasing energy, which would change the limits by ∼10% in both analyses. For the Razzaque et al. (2003b) supranova model we assume 445 bursts yr^{-1} (or $\frac{2}{3}$ of 666, the fraction of long duration bursts), *pp* neutrino generation below 2 PeV and p-γ above this energy. It should be noted that this supranova model is not well supported by observational data because it assumes a delay of ∼1 week to several months between the supernova and the GRB. Observations of supernovae associated with gamma-ray bursts, e.g., GRB 060218, have placed limits to this delay to be as small as a few hours (Campana et al. 2006). Model A of Murase & Nagataki (2006) assumes that the GRB rate is tied to star formation rate. We have also been provided (K. Murase &

[41] The model rejection factor is the multiplicative factor by which a predicted flux would need to be scaled in order to be ruled out by an analysis at a 90% confidence level.

[42] Note that it is also possible to base the normalization on the average photon fluence (as opposed to ultra–high energy cosmic rays) of $F_\gamma \sim 6\times10^{-6}$ ergs cm^{-2} and 666 bursts yr^{-1} as observed by BATSE. This results in a flux normalization of $A_{\nu_e+\nu_\mu+\nu_\tau} = 2.3\times10^{-9}$ GeV cm^{-2} s^{-1} sr^{-1} including all flavors and oscillations. This normalization takes into account the selection effects of BATSE.

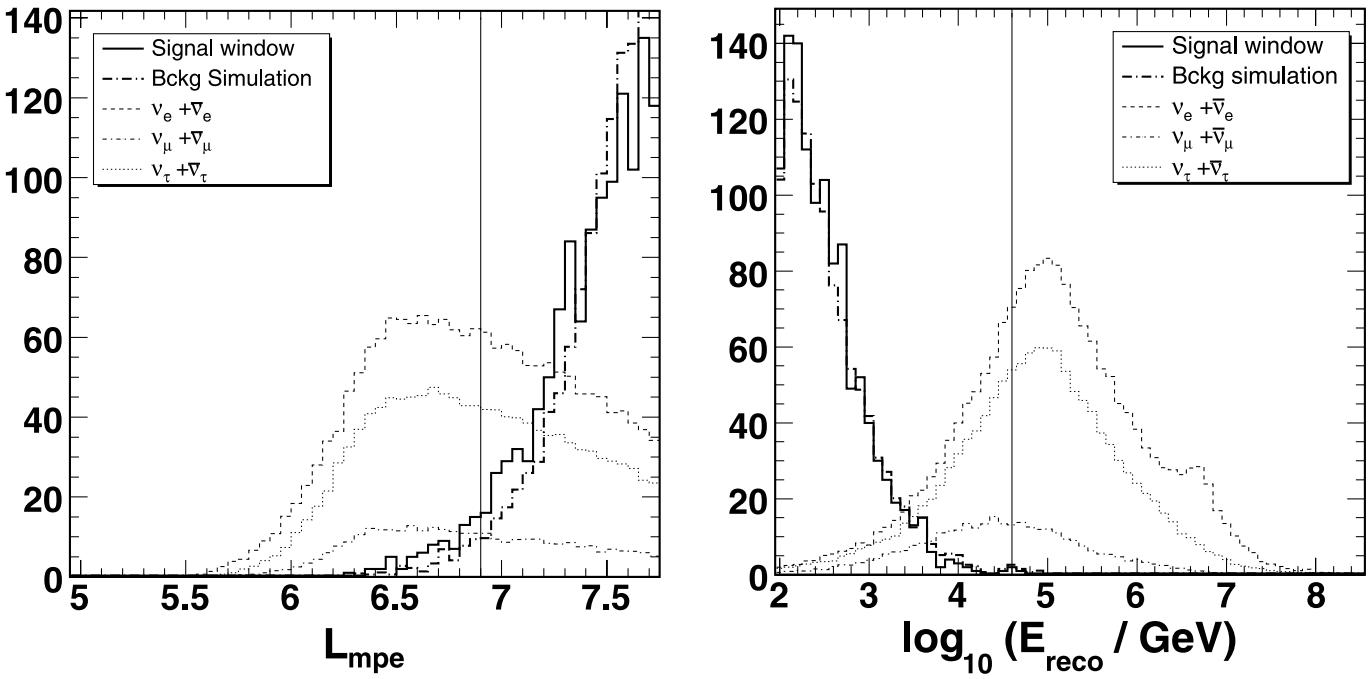

FIG. 6.—*Left*: Distribution of the likelihood parameter, $L_{\rm mpe}$. Data to the right of the vertical line are excluded. *Right*: Reconstructed cascade energy distribution, E_c. Data to the left of the vertical line are excluded. The signal simulation, following a Waxman-Bahcall spectrum, has been scaled up by a factor of 100,000. In both panels the vertical line corresponds to the final selection criteria. The background simulation has been scaled to match the number of events in the signal window.

S. Nagataki 2006, private communication) with the flux for the same model but for bursts following the redshift distribution of long duration BATSE-like bursts. In both analyses we use the latter distribution, which corresponds to a rate of 445 long-duration bursts $\rm yr^{-1}$. In practice, the difference in the predicted neutrino spectra in these two cases is very small. The model parameters used include a beamed energy per burst of 2×10^{51} ergs and the baryon loading factor is taken to be 100, a value which assumes GRBs are the primary source of cosmic rays. It should be noted that, since Murase & Nagataki (2006) model A is available for both electron and muon neutrino fluxes at the source, for this model these fluxes are used to calculate the flavor flux ratio at Earth taking into account full neutrino mixing. Because the electron and muon flux spectra are different, the flavor flux ratio at Earth is not strictly 1:1:1 for this model, but rather varies as a function of energy.

Limits for models that are not presented here can be tested by calculating:

$$N_{\rm expected} = T \int dE_\nu \, d\Omega \phi(E_\nu) A_{\rm eff}(E_\nu, \ \theta_\nu), \qquad (3)$$

where T is the exposure time, ϕ is the neutrino flux at the Earth's surface according to the model, $A_{\rm eff}$ is the effective area and $N_{\rm events}$ is the number of events predicted by the model. Given an expected number of events and the 90% c.l. upper signal event limit, N_{90}, the MRF for the model to be tested is

$$\mathrm{MRF} = \frac{N_{90}}{N_{\rm expected}}. \qquad (4)$$

Figures 7 and 8 show the neutrino effective area of AMANDA after all selection criteria for the rolling and the triggered analyses respectively have been applied.

7.1. *Rolling Analysis*

Upon unblinding the rolling analysis, the maximum number of events observed in any bin for the 1 s search was two, while the maximum in any bin in the 100 s search was three. These were the most likely outcomes of the analysis assuming no signal was present (with probabilities 70.2% and 75.4%, respectively, based on computer simulation). Further, the number of doublets and triplets, i.e., two or three events in a single time window, was very consistent with predictions assuming Poissonian statistics. The number of doublets in the 1 s search was 311 on an expected background of 310 ± 20. The number of doublets in the 100 s search was 1000 on an expected background of 1020 ± 30 and the number of triplets was 20 on an expected background of 22 ± 5.

Because this analysis looks for a cluster of temporally correlated events, it is not just the overall neutrino flux that determines the level at which we can observe a neutrino signal, but also the way that the neutrino flux is divided among discrete bursts. For example, it is statistically much more probable to obtain a cluster of several events from one very strong, nearby burst than from 100 bursts occurring at different times, even if the net neutrino fluxes at Earth for the two scenarios are equivalent. It is therefore necessary in this case to make an assumption about the relative distribution of neutrino events among all GRBs. Thus, the MRF for each model tested is determined using a signal simulation which varies the average expected neutrino flux by a random factor for each burst. These factors are weighted according to a Gaussian fit to the distribution of predicted event rates for individual GRBs from the BATSE catalog, which were obtained from Guetta et al. (2004). This accounts for several factors affecting neutrino flux, including distance from Earth and electromagnetic fluence. The majority of bursts therefore have a signal flux near the average rate while a few have either much higher or lower fluxes. The total year-long flux is thus divided into a number of unequal discrete bursts, with the number

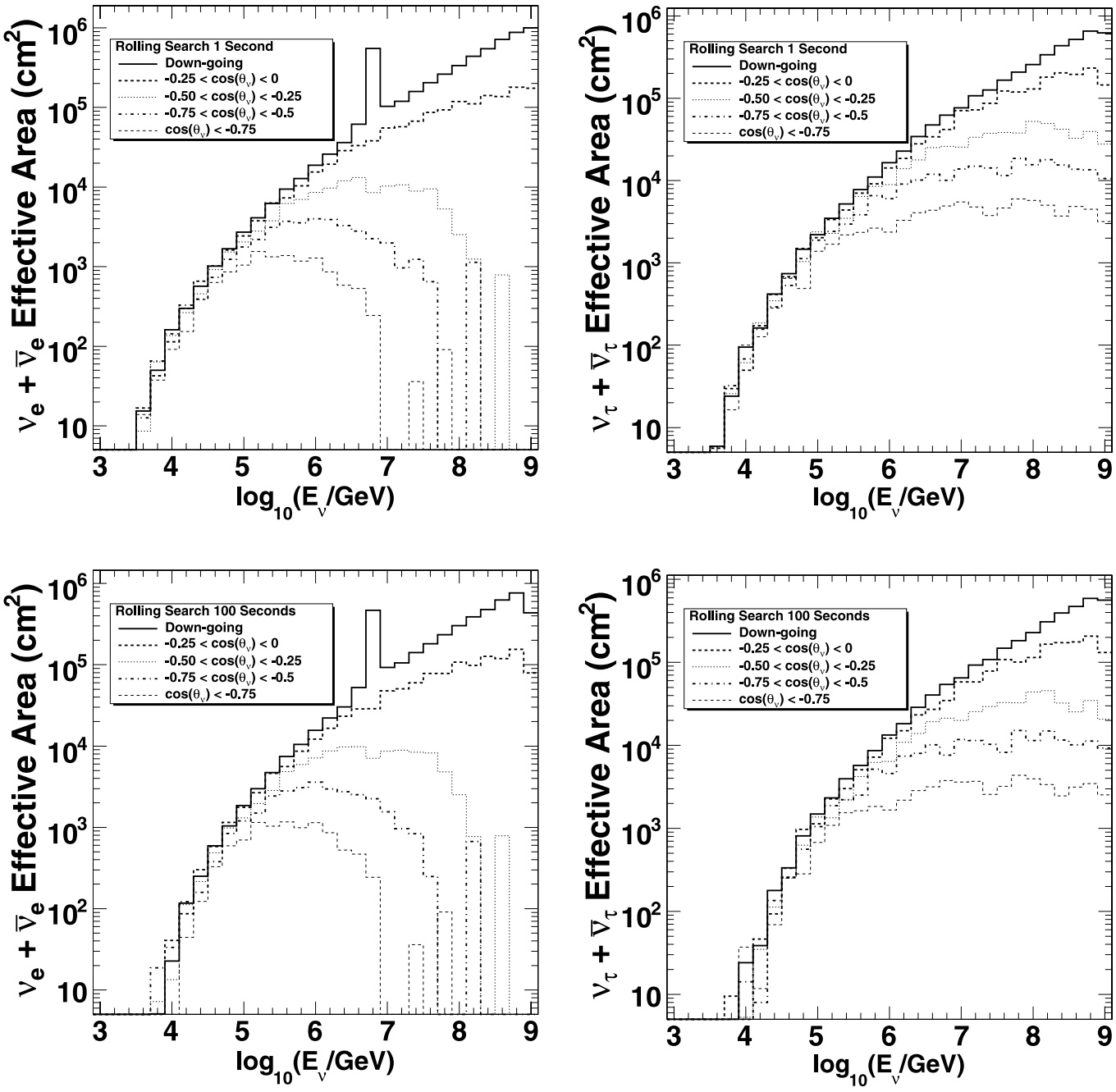

FIG. 7.—Neutrino effective areas as function of neutrino energy (at Earth surface) and cos θ_ν for the rolling analysis after all selection criteria have been applied, for both 1 and 100 s search windows. The peak at 6.3 PeV is due to the Glashow resonance for $\bar{\nu}_e$. The effective areas for ν_τ for up-going events are larger than for ν_e because of charged current regeneration. Effective areas for ν_μ and $\bar{\nu}_\mu$ are much smaller, because neutrino-induced cascades are produced via neutral current interactions only.

of bursts per year determined from the burst rate observed by BATSE.

The MRF for the Waxman-Bahcall method is 120 (100 without systematics), with 90% of events in the 70 TeV–8 PeV energy range. For this model, one-third of the bursts were assumed to be short (applied to both time windows) and two-thirds assumed to be long (applied to the 100 s time window only), with corrections made for the lower average fluence from short bursts relative to long bursts. The MRF relative to the Razzaque et al. (2003b) supranova model is 27, while relative to the Murase-Nagataki Model A flux, the MRF is 95. Since these models pertain only to long bursts, only the 100 s window was used for these models and the number of bursts per year was assumed to be 445.

One possible additional class of sources without direct photon signatures is choked bursts, which would emit precursor neutrinos like a conventional GRB, but have no gamma-ray emission or prompt neutrinos because the fireball never escapes from the interior of the stellar progenitor (Meszáros & Waxman 2001). The rolling analysis cuts are not optimized for the energy spectrum predicted for choked bursts, which peaks at a few TeV rather than ~100 TeV. The MRF calculated for this model is 72, assuming a choked burst rate 100 times greater than the rate of conventional GRBs (tied to the rate of Type II supernovae) and

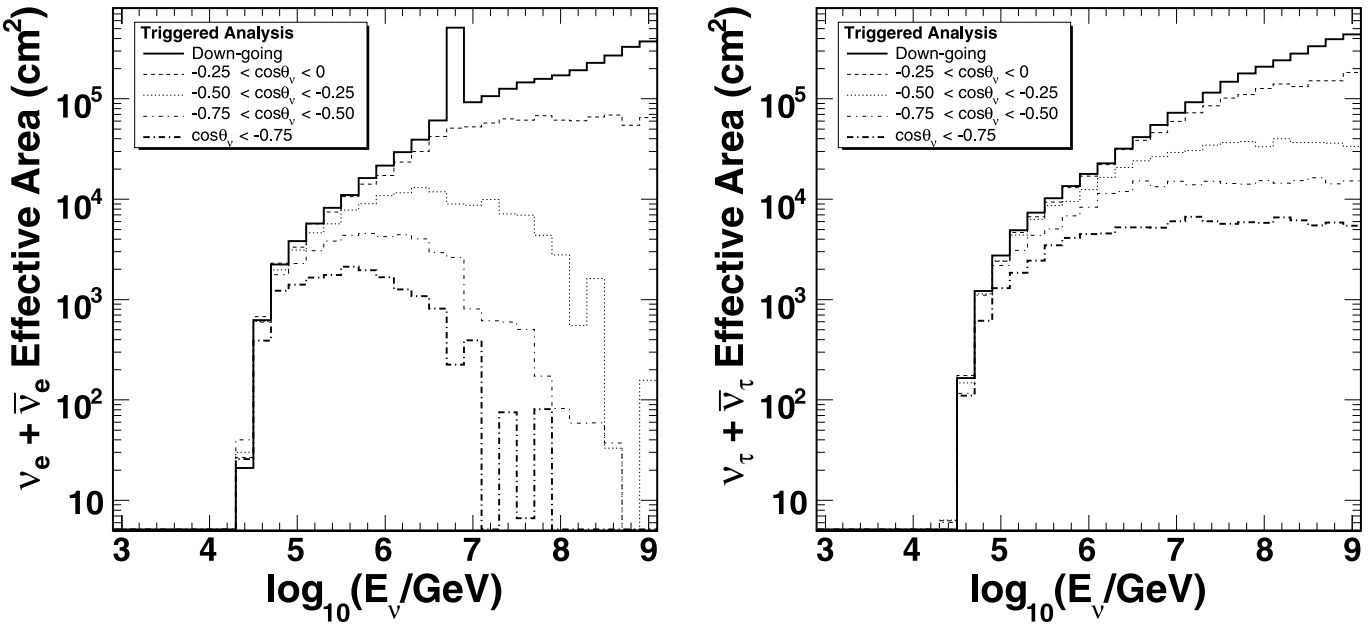

FIG. 8.—Neutrino effective areas as function of neutrino energy (at Earth surface) and cos θ_ν for the triggered analysis after all selection criteria have been applied. The peak at 6.3 PeV is due to the Glashow resonance for $\bar{\nu}_e$. The effective areas for ν_τ for up-going events are larger than for ν_e because of charged current regeneration.

assuming the progenitor to have an external hydrogen envelope (Razzaque et al. 2003a). Figure 9 and Table 4 summarize the limits presented here.

7.2. *Triggered Analysis*

After applying all selection criteria, for a simulated Waxman-Bahcall spectrum, we expect 0.03 events from 73 bursts. The final events sample is composed 55% by ν_e and $\bar{\nu}_e$, 7% by ν_μ and $\bar{\nu}_\mu$, and 38% by ν_τ and $\bar{\nu}_\tau$. The central 90% of the events from the Waxman-Bahcall flux are between 70 TeV and 8 PeV. Taking into account that the ratio of signal to off-time windows is 5.387×10^{-3}, we expected a background of $0.0054^{+0.013}_{-0.005}$.

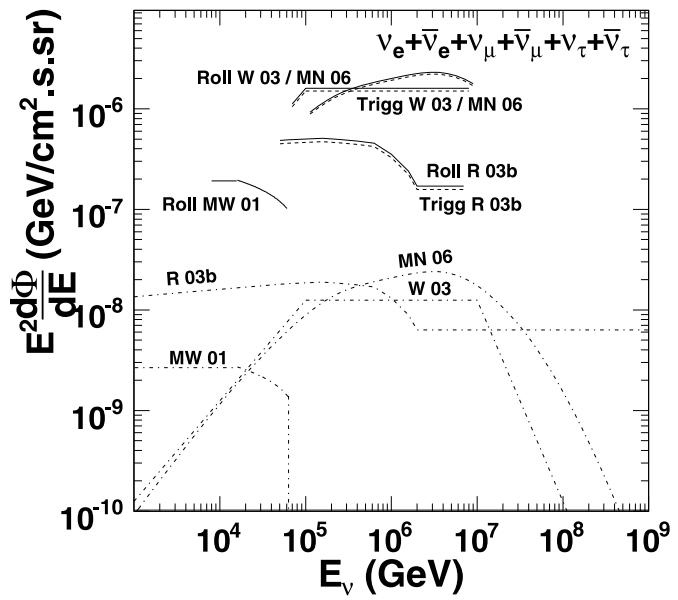

FIG. 9.—Predicted all-flavor diffuse neutrino fluxes and experimental limits. Models are shown by the dashed-dotted lines: Waxman (2003) (labelled "W 03,"); Razzaque et al. (2003b) ("R 03b,"); Murase & Nagataki (2006) model A ("MN 06,"); and Meszáros & Waxman (2001) ("MW 01,"). All theoretical predictions have been adjusted for vacuum oscillations. Also shown are the *rolling* search limits (labeled "Roll"; *solid line*) and *triggered* search limits (labeled "Trigg"; *dashed line*). [*See the electronic edition of the Journal for a color version of this figure.*]

After examination of the *signal* windows, no events are found in the combined 73 signal windows, so we find no evidence for neutrino induced-cascades in coincidence with GRBs reported by BATSE from 2000 February 13 to 2000 May 26. The signal event upper limit N_{90} is 3.5 (2.4 without systematics).

In order to determine what fraction of the total year-long isotropic neutrino flux comes from the bursts included in our sample, we simply divide the number of bursts studied by the expected total number of relevant bursts occurring per year. For the Waxman-Bahcall model, we have included both long duration GRBs and short duration GRBs, because the original model does not distinguish between the two classes. Thus, we assume our 73 burst sample contains 73/666, or 11%, of the year's total neutrino flux. The supranova and Murase-Nagataki models, however, apply only to long bursts. Since there are 53 long bursts in our sample and an expected rate of 445 long bursts per year, 12% of the total long burst neutrino flux is assumed to be contained in our burst sample.

The MRF for the Waxman-Bahcall model is 110 (78 without systematics). For the supranova model the expected signal after applying all selection criteria is 0.067 and the MRF, corrected by systematic uncertainties, is 25. For Murase-Nagataki model A we expect a signal of 0.0038 events. This signal expectation corresponds to a MRF of 94.

TABLE 4
MODEL REJECTION FACTORS

Model	Triggered Analysis	Rolling Analysis	Energy Range[a]
Waxman-Bahcall	110	120	70 TeV to 8 PeV
Razzaque et al.	25	27	50 TeV to 7 PeV
Murase-Nagataki (model A)	94	95	100 TeV to 10 PeV
Choked bursts	n/a	72	8 TeV to 61 TeV

[a] Relating to 90% of events.

8. CONCLUSIONS

We have performed two searches for neutrino-induced cascades with AMANDA-II. The triggered analysis searched for neutrinos in coincidence with 73 gamma-ray bursts reported by BATSE in 2000. The rolling analysis searched for a statistical excess of cascade-like events in time rolling windows of 1 and 100 s for the years 2001, 2002, and 2003. No evidence for neutrino-induced cascades from gamma-ray bursts is found. We present MRFs for the Waxman-Bahcall model, the supranova model, a choked-burst model and Murase & Nagataki Model A. For the Waxman-Bahcall model the MRF is 110 from the triggered analysis and 120 from the rolling analysis. At 1 PeV the triggered analysis limit is

$$E^2 \frac{d\Phi}{dE} \leq 1.5 \times 10^{-6}\ \mathrm{GeV\ cm^{-2}\ s^{-1}\ sr^{-1}}, \quad (5)$$

and the rolling analysis limit is

$$E^2 \frac{d\Phi}{dE} \leq 1.6 \times 10^{-6}\ \mathrm{GeV\ cm^{-2}\ s^{-1}\ sr^{-1}}. \quad (6)$$

Although there are advantages to the search methods discussed in this paper, our limits are not as constrictive as the muon neutrino limit, which lies at 1.7×10^{-8} GeV cm^{-2} s^{-1} sr^{-1} for the Waxman-Bahcall spectrum at 1 PeV (Achterberg et al. 2007). This value is for a single neutrino flavor only and should therefore be multiplied by a factor of $\sim$3 to obtain a more direct comparison to cascade all-flavor limits.

For the triggered analysis this difference is in large part due to the fact that the neutrino-induced muon search uses a much higher number of approximately 400 bursts reported between 1997 and 2003. Because the triggered analysis has a very low background rate the sensitivity should grow linearly with the number of bursts studied. Given the same set of bursts, the sensitivity of the triggered analysis is only a factor $\sim$4 worse than that of the neutrino-induced muon search. But, unlike the triggered up-going muon search, the triggered cascade analysis is sensitive to gamma-ray bursts in both the Southern and Northern Hemisphere. This can potentially double the sensitivity. In the case of the rolling analysis, the lack of spatial and temporal constraints results in a reduced per-burst sensitivity relative to triggered analyses, yet allows it to sample from a larger group of transients. This analysis therefore has the potential to detect sources missed by other methods. It thus serves as a useful complement to triggered GRB searches, especially during periods without large satellite experiments dedicated to GRB study. It should be noted that AMANDA searches for diffuse fluxes of extraterrestrial neutrinos using cascades (Ackermann et al. 2004; Ahrens et al. 2003b) can also be used to establish limits on neutrino emission by GRBs. But given the same exposure the analyses presented here have better sensitivity because time correlations significantly reduce the background.

Future searches with the AMANDA and IceCube detectors may include bursts reported by *Swift, GLAST*, and other IPN satellites. The capabilities of IceCube are particularly promising. Preliminary studies indicate that a triggered search for 300–500 bursts with IceCube would suffice to set limits at levels lower than predicted by Waxman-Bahcall or would find evidence of the existence of neutrinos in coincidence with GRBs with better than 5 σ confidence. Also, bursts that are particularly bright and close may result in signals that are strong enough to provide an unequivocal discovery from a single burst (Razzaque & Mezsáros 2004). If such a burst were to occur in the southern sky, only the cascade channel would be available to study this burst.

We are grateful for data provided and comments made by K. Murase. We acknowledge the support from the following agencies: National Science Foundation (Office of Polar Program; Physics Division), University of Wisconsin Alumni Research Foundation, Department of Energy, and National Energy Research Scientific Computing Center (supported by the Office of Energy Research of the Department of Energy), the NSF-supported TeraGrid system at the San Diego Supercomputer Center (SDSC), and the National Center for Supercomputing Applications (NCSA); Swedish Research Council, Swedish Polar Research Secretariat, and Knut and Alice Wallenberg Foundation, Sweden; German Ministry for Education and Research, Deutsche Forschungsgemeinschaft (DFG), Germany; Fund for Scientific Research (FNRS-FWO), Flanders Institute to encourage scientific and technological research in industry (IWT), Belgian Federal Office for Scientific, Technical and Cultural affairs (OSTC); the Netherlands Organisation for Scientific Research (NWO); M. R. acknowledges the support of the SNF (Switzerland); J. D. Z. acknowledges the Marie Curie OIF Program (contract 007921).

REFERENCES

Achterberg, A., et al. 2007, ApJ, submitted (astro-ph/07051186)
Ackermann, M., et al. 2004, Astropart. Phys., 22, 127
———. 2005, Proc. 29th Int. Cosmic Ray Conf. (Pune), (astro-ph/0509330)
———. 2006, J. Geophys. Res., 111, D13203
Ahrens, J., et al. 2003a, Phys. Rev. D, 67, 012003
———. 2003b, Phys. Rev. Lett., 90, 251101
———. 2004, Nucl. Instr. Meth. A, 524, 169
Andrés E., et al. 2001, Nature, 410, 441
Athar, H., Kim, C. S., & Lee, J. 2006, Mod. Phys. Lett. A, 21, 1049
Bay, R. 2000, Ph.D. thesis, Univ. California, Berkeley
Campana, S., et al. 2006, Nature, 442, 1008
Chirkin, D., & Rhode, W. 2001, preprint (hep-ph/0407075)
Conrad, J., Botner, O., Hallgren, A., & Pérez de los Heros, C. 2002, Phys. Rev. D, 67, 012002
Feldman, G. J., & Cousins, R. D. 1998, Phys. Rev. D, 57, 3873
Gandhi, R., et al. 1999, Phys. Rev. D, 58, 093009
Gazizov, A., & Kowalski, M. 2005, Comput. Phys. Commun., 172, 203
Guetta, D., et al. 2004, Astropart. Phys. 20, 429
Hardtke, R. 2002, Ph.D. thesis, Univ. Wisconsin
Heck, D. 1998, Tech. Rep. FZKA-6019 (Karlsruhe: Forschungszentrum Karlsruhe)
Hill, G. C. 2003, Phys. Rev. D, 67, 118101
Hill, G. C., & Rawlins, K. 2003, Astropart. Phys., 19, 393
Hill, G. C., et al. 2005, in Proc. PHYSTAT 2005, ed. L. Lyons & M. K. Unel (Oxford: Imperial College Press)
Hundertmark, S. 1998, in Methodical Aspects of Underwater/Ice Neutrino Telescopes (Zeuthen: DESY), 69
Jakobsson, P., et al. 2005, A&A, 447, 897
Joachims, T. 1999, Making Large-Scale SVM Learning Practical (Cambridge: MIT Press)
Kashti, T., & Waxman, E. 2005, Phys. Rev. Lett., 95, 181101
Kowalski, M. 2004, Ph.D. thesis, Humboldt Univ., Berlin
Kuehn, K., et al. 2005, in Proc. 29th Int. Cosmic Ray Conf. (Pune) (astro-ph/0509330)
Learned, J., & Pakvasa, S. 1995, Astropart. Phys., 3, 267
Maltoni, M., et al. 2004, New, J. Phys., 6, 122
Mezsáros, P., & Rees, M. J. 1994, MNRAS 269, 41P
Mezsáros, P., & Waxman, E. 2001, Phys. Rev. Lett., 87, 171102
Murase, K., & Nagataki, S. 2006, Phys. Rev. D, 73, 063002
Paciesas, W. S., et al. 1999, ApJS, 122, 465
Paczynski, B., & Xu, G. 1994, ApJ, 427, 708
Piran, T. 2005, Rev. Mod. Phys., 76, 1143

Pohl, A. C. 2004, Lic. thesis, Kalmar Univ.
Razzaque, S., & Mezsáros, P. 2004, Phys. Rev. D, 69, 023001
Razzaque, S., Meszáros, P., & Waxman, E. 2003a, Phys. Rev. D, 68, 083001
———. 2003b, Phys. Rev. Lett., 90, 241103
Stamatikos, M., et al. 2005, in Proc. 29th Int. Cosmic Ray Conf. (Pune) (astro-ph/0510336)
Taboada, I. 2002, Ph.D. thesis, Univ. Pennsylvania
Waxman, E. 1995, Phys. Rev. Lett., 75, 386
———. 2003, Nucl. Phys. Proc. Suppl., 118, 353
Waxmann, E., & Bahcall, J. 1997, Phys. Rev. Lett., 78, 2292
———. 2000, ApJ, 541, 707
Wick, S., Dermer, C. D., & Atoyan, A. 2004, Astropart. Phys., 21, 125
Yao, W. M., et al. 2006, J. Phys. G33, 1
Zhang, B., & Meszáros, P. 2004, Int. J. Mod. Phys., A19, 2385